1894 *Inorg. Chem.* **2010**, *49*, 1894–1904
DOI: 10.1021/ic902244m

Inorganic Chemistry
Article

Hybrid Organic/Inorganic Complexes Based on Electroactive Tetrathiafulvalene-Functionalized Diphosphanes Tethered to C_3-Symmetrized Mo_3Q_4 (Q = S, Se) Clusters

Narcis Avarvari,[†] Kaplan Kiracki,[‡] Rosa Llusar,*[,‡] Victor Polo,[§,∥] Ivan Sorribes,[‡] and Cristian Vicent*[,⊥]

[†]*Université d'Angers, CNRS, Laboratoire de Chimie et Ingénierie Moléculaire, CIMA UMR 6200, UFR Sciences, Bât. K, 2 Bd. Lavoisier, 49045 Angers, France,* [‡]*Departament de Química Física i Analítica, Universitat Jaume I, Av. Sos Baynat s/n, 12071 Castelló, Spain,* [§]*Instituto de Biocomputación y Física de los Sistemas Complejos (BIFI), Edificio Cervantes, Corona de Aragón 42, Zaragoza 50009, Spain,* [∥]*Departamento de Química Orgánica y Química Física, Universidad de Zaragoza, c/ Pedro Cerbuna s/n, 50009 Zaragoza, Spain, and* [⊥]*Serveis Centrals d'Instrumentació Científica, Universitat Jaume I, Av. Sos Baynat s/n, 12071 Castelló, Spain*

Received November 13, 2009

A two-step procedure for the preparation of hybrid complexes based on electroactive tetrathiafulvalene (TTF)-functionalized *o*-P_2 diphosphanes (*o*-P_2 = 3,4-dimethyl-3,4-bis(diphenylphosphino)tetrathiafulvalene) and inorganic C_3-symmetrized Mo_3Q_4 (Q = S, Se) clusters, namely, $[Mo_3S_4Cl_3(o\text{-}P_2)_3]PF_6$ ([**1**]PF_6) and $[Mo_3Se_4Cl_3(o\text{-}P_2)_3]PF_6$ ([**2**]PF_6), is reported. Their molecular and electronic structures are also described on the basis of X-ray diffraction experiments and density functional theory (DFT) calculations aimed at understanding the interactions established between both the organic and the inorganic parts. Cyclic voltammograms of compounds [**1**]PF_6 and [**2**]PF_6 display reduction features associated to the Mo_3Q_4 core and oxidation characteristics due to the TTF skeleton. The oxidation chemistry of [**1**]PF_6 and [**2**]PF_6 in solution is also investigated by means of in situ electrospray ionization (ESI) mass spectrometry, UV−vis, and, electron paramagnetic resonance (EPR) measurements. Upon addition of increasing amounts of $NOPF_6$ (less than 3 equiv), the sequential formation of $\mathbf{1}^{n+}$ (n = 1−4) species was observed whereas addition of a 3-fold excess of $NOPF_6$ allows to access the three-electron oxidized $[Mo_3S_4Cl_3(o\text{-}P_2)_3]^{4+}$ ($\mathbf{1}^{4+}$) and $[Mo_3Se_4Cl_3(o\text{-}P_2)_3]^{4+}$ ($\mathbf{2}^{4+}$) cations. These $\mathbf{1}^{4+}$ and $\mathbf{2}^{4+}$ cations represent still rare examples of complexes with oxidized TTF-ligands that are remarkably stable either toward diphosphane dissociation or phosphane oxidation. Polycrystalline samples of compound [**1**]$(PF_6)_4$ were obtained by oxidation of compound [**1**]PF_6 using $NOPF_6$ which were analyzed by solid state absorption, UV−vis, and Raman spectroscopies.

Introduction

The co-assembly of cationic donor tetrathiafulvalene (TTF) derivatives and metal-containing anions has been extensively investigated aimed at preparing hybrid inorganic/organic materials which can introduce multifunctionality (for example by combining a conducting organic network with an inorganic magnetic component) in the resulting molecular compound.[1] Another way to construct molecular organic−inorganic hybrids based on organic TTF donors and inorganic moieties relies on the covalent association of both components in one building block.[2] This goal can be accomplished through the functionalization of the TTF core with substituents capable of coordinating a metallic center, such as thiolates,[3] phosphanes,[4−11] acetylacetonates,[12] or

*To whom correspondence should be addressed. E-mail: barrera@sg.uji.es (C.V.), rosa.llusar@qfa.uji.es (R.L.).

(1) (a) Ouahab, L.; Batail, P.; Perrin, C.; Garrigou-Lagrange, C. *Mater. Chem. Bull.* **1986**, *21*, 1223. (b) Penicaud, A.; Batail, P.; Davidson, P.; Levelut, A. M.; Coulon, C.; Perrin, C. *Chem. Mater.* **1990**, *2*, 117. (c) Kurmoo, M.; Graham, A. W.; Day, P.; Coles, S. J.; Hursthouse, M. B.; Caulfield, J. L.; Singleton, J.; Pratt, F. L.; Hayes, W.; Ducasse, L.; Guionneau, P. *J. Am. Chem. Soc.* **1995**, *117*, 12209. (d) Coronado, E.; Galán-Mascarós, J. R.; Gómez-Garcķa, C.; Laukhin, V. *Nature* **2000**, *408*, 447. (e) Rashid, S.; Turner, S. S.; Day, P.; Howard, J. A. K.; Guionneau, P.; McInnes, E. J. L.; Mabbs, F. E.; Clark, R. J. H.; Firth, S.; Biggs, T. *J. Mater. Chem.* **2001**, *11*, 2095. (f) Gabriel, J. C. P.; Boubekeur, K.; Uriel, S.; Batail, P. *Chem. Rev.* **2001**, *101*, 2037. (g) Deluzet, A.; Rousseau, R.; Guilbaud, C.; Granger, I.; Boubekeur, K.; Batail, P.; Canadell, E.; Auban-Senzier, P.; Jerome, D. *Chem.—Eur. J.* **2002**, *8*, 3884. (h) Coronado, E.; Day, P. *Chem. Rev.* **2004**, *104*, 5419. (i) Fourmigue, M.; Batail, P. *Chem. Rev.* **2004**, *104*, 5379.

(2) Lorcy, D.; Bellec, N.; Fourmigue, M.; Avarvari, N. *Coord. Chem. Rev.* **2009**, *253*, 1398.

(3) Kobayashi, H.; Fujiwara, H.; Kobayashi, A. *Chem. Rev.* **2004**, *104*, 5243.

(4) Fourmigue, M.; Uzelmeier, C. E.; Boubekeur, K.; Bartley, S. L.; Dunbar, K. R. *J. Organomet. Chem.* **1997**, *529*, 343.

(5) Uzelmeier, C. E.; Bartley, S. L.; Fourmigue, M.; Rogers, R.; Grandinetti, G.; Dunbar, K. R. *Inorg. Chem.* **1998**, *37*, 6706.

(6) Avarvari, N.; Martin, D.; Fourmigue, M. *J. Organomet. Chem.* **2002**, *643−644*, 292.

(7) Devic, T.; Batail, P.; Fourmigue, M.; Avarvari, N. *Inorg. Chem.* **2004**, *43*, 3136.

(8) Avarvari, N.; Fourmigue, M. *Chem. Commun.* **2004**, 1300.

Published on Web 01/19/2010

Scheme 1. Schematic Drawn at Approximately the Same Scale of Re_6Se_8, W_6S_8, and Mo_3S_4 Clusters Together with the Phosphane Coordination Mode (Mono- or Diphosphane)

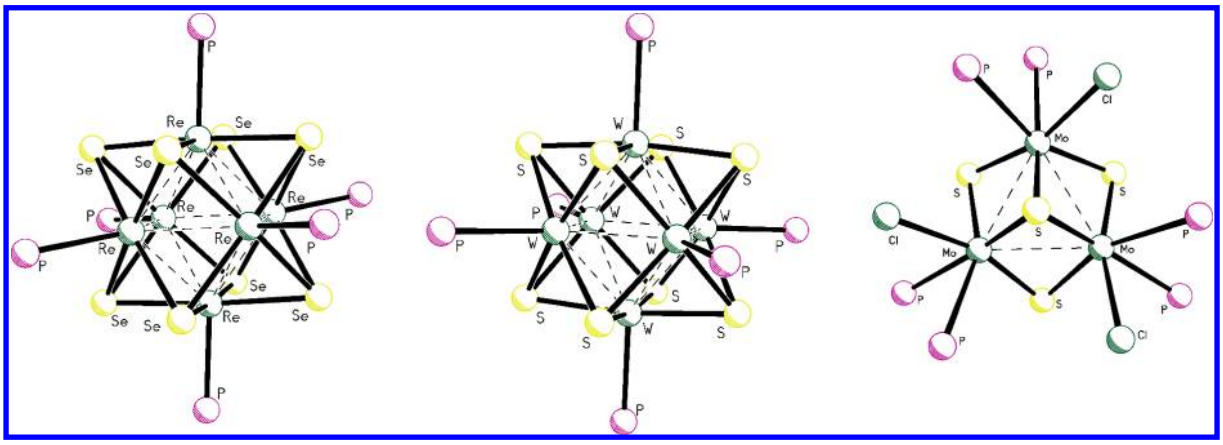

pyridines.[13,14] The role of the inorganic part is important in directing the orientation and assembly of its coordinated TTF-functionalized ligands in a predetermined way as dictated by its coordination number and inherent geometry. In this context, besides the use of mononuclear metal centers, the use of molecular metal clusters as platforms for the assembly of electroactive TTF units represents a promising alternative because of their large size combined with their rich coordination chemistry and structural and electronic diversity, which may produce novel synergistic effects between the organic and the inorganic parts, leading to new physicochemical properties.

TTF-functionalized phosphanes represent a family of electroactive TTF-based ligands which possess the ability to coordinate to a large variety of metal centers. From a synthetic point of view, the coordination chemistry of the TTF-functionalized phosphanes to either mono- or polynuclear species is expected to be easily paralleled from that previously reported for the non-TTF-functionalized phosphanes. For example, precedence for mononuclear compounds containing TTF (or dithiafulvalene)-functionalized mono- (P) or diphosphanes (P−P) exists in the form of $[M(P-P)Cl_2]$ (M = Ni,[15] Pd, Pt[7]), $[M(P-P)_2]^{+,2+}$ (M = Rh,[4] Cu, Ag,[9,16] Fe, Co, Ni, Pd and Pt[16]) complexes as well as some low-valent metal carbonyl compounds of Mo and W,[11,17,18] Mn,[18] Ru,[19] Fe,[6,19] and Re[6] by adaptation of the synthetic procedure developed for the non-TTF-functionalized phosphanes. Regarding cluster-based complexes, octahedral chalcogen face-capped Re_6Se_8[20] and W_6S_8,[21] cluster units with terminal phosphane ligands are known. To the best of our knowledge, Re_6Se_8 and W_6S_8 units have been the first cluster cores used as coordination sites for TTF-containing phosphane ligands.

These octahedrally symmetrized Re_6Se_8 and W_6S_8 clusters display several structural and electronic features different from that found in mononuclear complexes; among them, the wide orientation possibilities of the TTF ligands, the high overall number of electrons delivered upon TTF-based oxidation, as well as the rich electrochemistry displayed by the cluster cores. Hence, the octahedrally symmetrized $W_6S_8((TTF)PEt_2)_6$ and $Re_6Se_8((Me_2TTF)PPh_2)_6$ clusters may incorporate at least six electron donor moieties delivering up to 12 electrons (or twelve donor units in $W_6S_8((TTF)_2PEt)_6$, and $Re_6Se_8((Me_2TTF)_2PPh)_6$, delivering up to 24 electrons) accompanied by electrochemical features associated to the cluster cores (for example, one oxidation and two reduction waves at $E_{1/2}$ = 0.12, −0.9, and −1.0 (vs Ag/AgCl) typically found in W_6S_8 clusters).[22] These examples illustrate that the use of molecular forms of metallic clusters as platforms for the assembly of several TTF units holds much promise for the straightforward access toward multidimensional precursors and prompted us to seek new cluster topologies for TTF-based ligand coordination.

In the past years, our group has been involved in the preparation of group VI chalcogenides featuring a Mo_3Q_4 (Q = S, Se) core decorated with diphophanes.[23−25] The trinuclear Mo_3Q_4 cluster unit is formed by three molybdenum atoms defining an equilateral triangle, one capping and three bridging

(9) Smucker, B. W.; Dunbar, K. M. *J. Chem. Soc., Dalton Trans.* **2000**, 1309.
(10) Cerrada, E.; Diaz, C.; Diaz, M. C.; Hursthouse, M. B.; Laguna, M.; Light, M. E. *Dalton Trans.* **2002**, 1104.
(11) Pellon, P.; Gachot, G.; Le Bris, J.; Marchin, S.; Carlier, R.; Lorcy, D. *Inorg. Chem.* **2003**, *42*, 2056.
(12) Massue, J.; Bellec, N.; Chopin, S.; Levillain, E.; Roisnel, T.; Clérac, R.; Lorcy, D. *Inorg. Chem.* **2005**, *44*, 8740.
(13) (a) Iwahori, F.; Gohlen, S.; Ouahab, L.; Carlier, R.; Sutter, J.-P. *Inorg. Chem.* **2001**, *40*, 6541. (b) Setifi, F.; Ouahab, L.; Golhen, S.; Yoshida, Y.; Saito, G. *Inorg. Chem.* **2003**, *42*, 1791.
(14) (a) Liu, S.-X.; Dolder, S.; Franz, P.; Neels, A.; Stoeckli-Evans, H.; Decurtins, S. *Inorg. Chem.* **2003**, *42*, 4801. (b) Devic, T.; Avarvari, N.; Batail, P. *Chem.—Eur. J.* **2004**, *10*, 3697.
(15) Fourmigue, M.; Batail, P. *Bull. Soc. Chim. Fr.* **1992**, *129*, 829.
(16) Uzelmeier, C. E.; Smucker, B. W.; Reinheimer, E. W.; Shatruk, M.; O'Neal, A. W.; Fourmigue, M.; Dunbar, K. R. *Dalton Trans.* **2006**, 5259.
(17) (a) Guerro, M.; Roisnel, T.; Pellon, P.; Lorcy, D. *Inorg. Chem.* **2005**, *44*, 3347. (b) Gachot, G.; Pellon, P.; Roisnel, T.; Lorcy, D. *Eur. J. Inorg. Chem.* **2006**, 2604.
(18) Guerro, M.; Di Piazza, E.; Jiang, X.; Roisnel, T.; Lorcy, D. *J. Organomet. Chem.* **2008**, *693*, 2345.
(19) Gouverd, C.; Biaso, F.; Cataldo, L.; Berclaz, T.; Geoffroy, M.; Levillain, E.; Avarvari, N.; Fourmigue, M.; Sauvage, F. X.; Wartelle, C. *Phys. Chem. Chem. Phys.* **2005**, *7*, 85.
(20) Perruchas, S.; Avarvari, N.; Rondeau, D.; Levillain, E.; Batail, P. *Inorg. Chem.* **2005**, *44*, 3459.
(21) Yuan, M.; Ülgut, B.; McGuire, M.; Takada, K.; DiSalvo, F. J.; Lee, S.-K.; Abruña, H. *Chem. Mater.* **2006**, *18*, 4296.
(22) (a) Saito, T.; Yoshikawa, A.; Yamagata, T.; Imoto, H.; Unouora, K. *Inorg. Chem.* **1989**, *28*, 3588. (b) Venkataraman, D.; Rayburn, L. L.; Hill, L. I.; Jin, S.; Malik, A.-S.; Turneau, K. J.; DiSalvo, F. J. *Inorg. Chem.* **1999**, *38*, 828.
(23) Estevan, F.; Feliz, M.; Llusar, R.; Mata, J. A.; Uriel, S. *Polyhedron* **2001**, *20*, 527.
(24) Llusar, R.; Uriel, S.; Vicent, C. *J. Chem. Soc., Dalton Trans.* **2001**, 2813.
(25) Feliz, M.; Llusar, R.; Uriel, S.; Vicent, C.; Humphrey, M. G.; Lucas, N. T.; Samoc, M.; Luther-Davies, B. *Inorg. Chim. Acta* **2003**, *349*, 69.

Scheme 2

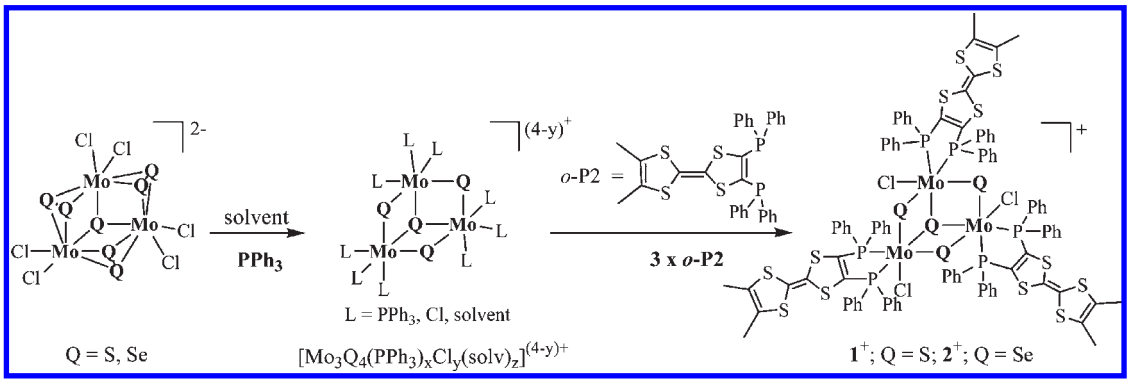

chalcogen ligands. For comparative purposes, Scheme 1 shows a schematic representation of the Re_6Se_8 and W_6S_8 clusters for which TTF-phosphanes have been coordinated, together with Mo_3Q_4 clusters investigated herein.

Chelating diphosphanes such as bis(dimethylphosphino)-ethane (dmpe) or bis(diphenylphosphino)-ethane (dppe) are widely used for the stabilization of Mo_3Q_4 (Q = S, Se) cluster complexes.[23,24] With regard to TTF-functionalized ligands that parallel dmpe or dppe chemistry, the phosphorus substituted tetrathiafulvalene molecule, *o*-$(CH_3)_2(PPh_2)_2$TTF (*o*-P_2, see Scheme 2)[15] is a rational choice. However, *o*-P_2 coordination chemistry to polynuclear complexes has been scarcely explored, the only example reported to date being the reaction of $[Re_2Cl_8]^{2-}$ with *o*-P_2 in refluxing ethanol to yield the mixed-nuclearity salt $[ReCl_2(o\text{-}P_2)_2][Re_2Cl_6(o\text{-}P_2)]$.[5] By analogy with Mo_3Q_4 clusters featuring dmpe or dppe ligands (see Scheme 1), coordination of *o*-P_2 to Mo_3Q_4 clusters would necessarily imply the bidentate coordination of these TTF-based diphosphanes at the outer positions of the Mo sites, thus generating hybrid organic/inorganic C_3-symmetrized Mo_3Q_4 clusters that offers an alternative to the purely organic C_3-symmetrized multi-TTF donor molecules.[26] Herein, we investigate the covalent association of the electroactive TTF-based diphosphane ligand *o*-P_2 to the inorganic Mo_3Q_4 cluster cores and the structural, electronic, electrochemical properties as well as oxidation chemistry of the new hybrid molecular complexes both in solution and in solid state.

Experimental Section

Physical Measurements. $^{31}P\{^1H\}$ NMR spectra were recorded on Varian MERCURY 300 MHz spectrometer, using CD_2Cl_2 as a solvent and are referenced to external 85% H_3PO_4. Raman spectra were recorded on polycrystalline samples with a JASCO NRS 3100 Laser Raman using a He−Ne laser source at 632.8 nm. The laser beam was focused by a microscope equipped with a 20× lens and a spot diameter of 0.2 mm. The power at the surface sample was set to about 50 mW. For the Se-containing sample, namely, [**2**]PF_6, the power at the surface sample was carefully adjusted at about 1 mW to avoid overheating or burning up processes. Elemental analyses were carried out on a EuroEA3000 Eurovector Analyzer. Electrospray mass spectra were recorded on a Q-TOF I instrument (Waters, Manchester) using CH_2Cl_2:CH_3CN as solvent. A capillary voltage of 3.5 KV was used in the positive scan mode, and the cone voltage (U_c) was set to 15 V to control the extent of fragmentation of the identified ions. Oxidation reactions of compounds [**1**]PF_6 and [**2**]PF_6 using different oxidants were monitored by electrospray ionization-mass spectrometry (ESI-MS). Typically, after mixing acetonitrile solutions of clusters [**1**]PF_6 or [**2**]PF_6 and dichloromethane methanol solutions of $NOPF_6$, a drop of the solution was extracted, diluted in acetonitrile, and a positive-ion mass spectrum collected. The oxidation reaction immediately reached the equilibrium since variations in chemical speciation were not observed after the addition of the oxidant. The chemical composition of each peak was assigned by comparison of the isotope experimental pattern with that calculated using the MassLynx 4.1 program. Cyclic voltammetry experiments were performed with a Echochemie Pgstat 20 electrochemical analyzer. All measurements were carried out with a conventional three-electrode configuration consisting of platinum working and auxiliary electrodes and a Ag/AgCl reference electrode containing aqueous 3 M KCl. The solvent used in all experiments was CH_2Cl_2 (Merck HPLC grade). The supporting electrolyte was 0.1 M tetrabutylammonium hexafluorophosphate. $E_{1/2}$ values were determined as $1/2\,(E_a + E_c)$, where E_a and E_c are the anodic and cathodic peak potentials, respectively. EPR spectra have been recorded on a Bruker 300 spectrometer (X-band). Electrochemical oxidations were carried out in situ in the EPR cavity using a two-electrodes cell; solutions in tetrahydrofuran (THF, 10^{-6} M) were carefully dried and degassed, and ammonium hexafluorophosphate (0.1 M) was used as supporting electrolyte. Sample tubes for the study of chemical oxidation products were prepared inside a glovebox.

General Procedures. All reactions were carried out under a nitrogen atmosphere using standard Schlenck techniques. The polymeric phases $\{Mo_3Q_7Cl_4\}_n$ (Q = S, Se),[27,28] molecular $(n\text{-}Bu_4N)_2[Mo_3S_7Cl_6]$[29] and $(PPh_4)_2[Mo_3Se_7Cl_6]$,[28] and the *o*-P_2 ligand were prepared according to literature methods.[15] The remaining reactants were obtained from commercial sources and used as received. Solvents for synthesis were dried and degassed by standard methods before use.

Synthesis. **$[Mo_3S_4Cl_3(o\text{-}P_2)_3]PF_6$ ([1]PF_6).** To an orange suspension of $(Bu_4N)_2[Mo_3S_7Cl_6]$ (47 mg, 0.039 mmol) in CH_3OH (10 mL) was added a 5-fold-excess of PPh_3 (51 mg, 0.195 mmol) under nitrogen. The color of the solution turns green immediately. After 2 h, *o*-P_2 (117 mg, 0.195 mmol) was added, and the solution was stirred overnight at room temperature

(26) (a) Fourmigue, M.; Johansen, I.; Boubekeur, K.; Nelson, C.; Batail, P. *J. Am. Chem. Soc.* **1993**, *115*, 3752. (b) Blanchart, P.; Svenstrup, N.; Rault-Berthelot, J.; Riou, A.; Becher, J. *Eur. J. Org. Chem.* **1998**, 1743. (c) Gonzalez, A.; Segura, J. L.; Martin, N. *Tetrahedron Lett.* **2000**, *41*, 3083. (d) Hasegawa, M.; Takano, J.-i.; Enozawa, H.; Kuwatani, Y.; Iyoda, M. *Tetrahedron Lett.* **2004**, *45*, 4109. (e) Danila, I.; Riobé, F.; Puigmartķ-Luis, J.; Pérez del Pino, A.; Wallis, J. D.; Amabilino, D.; Avarvari, N. *J. Mater. Chem.* **2009**, *19*, 4495.

(27) Fedin, V. P.; Sokolov, M. N.; Gerasko, O.; Kolesov, B. A.; Fedorov, V. Y.; Mironov, Y. V.; Yufit, D. S.; Slovohotov, Y. L.; Struchkov, Y. T. *Inorg. Chim. Acta* **1990**, *175*, 217.

(28) Fedin, V. P.; Sokolov, M. N.; Gerasko, A. O.; Virovets, A. V.; Podberezskaya, N. V.; Fedorov, V. Y. *Inorg. Chim. Acta* **1991**, *187*, 81.

(29) Fedin, V. P.; Sokolov, M. N.; Fedorov, V. Y.; Yufit, D. S.; Struchkov, Y. T. *Inorg. Chim. Acta* **1991**, *179*, 35.

Table 1. Crystallographic Data for *o*-Ps=S, $[Mo_3S_4Cl_3(o\text{-}P_2)_3]PF_6\cdot 2CH_2Cl_2$ (**1**·$2CH_2Cl_2$) and $[Mo_3Se_4Cl_3(o\text{-}P_2)_3]\cdot CH_2Cl_2\cdot C_4H_{10}O$ (**2**·$CH_2Cl_2\cdot C_4H_{10}O$)

compound	*o*-P_2=S	**1**·$2CH_2Cl_2$	**2**·$CH_2Cl_2\cdot C_4H_{10}O$
empirical formula	$C_{32}H_{26}P_2S_5$	$C_{98}H_{82}C_{17}F_6Mo_3P_7S_{16}$	$C_{101}H_{90}Cl_5F_6Mo_3OP_7S_{12}Se_4$
formula weight	632.77	2639.36	2816.15
crystal system	triclinic	triclinic	triclinic
a, Å	10.604(2)	14.068(3)	14.126(2)
b, Å	12.096(3)	17.676(4)	17.742(3)
c, Å	14.241(3)	26.844(6)	27.004(4)
α, deg	65.76(2)	96.714(5)	97.207(3)
β, deg	71.15(2)	105.056(4)	104.872(3)
γ, deg	70.89(2)	112.660(4)	112.674(3)
V, Å^3	1535.6(5)	5770(2)	5841.3(15)
T, K	293(2)	223(2)	223(2)
space group	$P\bar{1}$	$P\bar{1}$	$P\bar{1}$
Z	2	2	2
μ(Mo Kα), mm^{-1}	0.503	0.923	2.042
reflections collected	10387	32176	33031
ϕ range for data collection	1.90 to 22.50	0.81 to 25.00	0.81 to 25.00
unique reflections/*R*(int)	3816 [*R*(int) = 0.1822]	20297 [*R*(int) = 0.0602]	20542 [*R*(int) = 0.0305]
goodness-of-fit on F^2	0.810	1.186	1.159
R1[a]/wR2[b]	R1 = 0.0644	R1 = 0.0778	R1 = 0.0500
	wR2 = 0.1240	wR2 = 0.2030	wR2 = 0.1453
	R1 = 0.1865	R1 = 0.1449	R1 = 0.0775
	wR2 = 0.1580	wR2 = 0.2387	wR2 = 0.1609
residual ρ/e A^{-3}	0.445 and −0.317	2.761 and −1.861	1.289 and −0.863

[a] $R1 = \sum||F_o| - |F_c||/\sum|F_o|$. [b] $wR2 = [\sum w(F_o^2 - F_c^2)^2/\sum w(F_o^2)^2]^{1/2}$.

to give an orange slurry. After evaporation of the solvent, the resulting orange precipitate was redissolved in CH_2Cl_2, filtered and adsorbed onto a silica gel column. After washing of the column with acetone, elution with a KPF_6 solution in acetone (1 mg/mL) afforded a very concentrated orange solution. This solution was taken to dryness, redissolved in CH_2Cl_2, and filtered to remove the insoluble KCl or KPF_6 inorganic salts. Finally, an air stable microcrystalline orange-brown solid, characterized as $[Mo_3S_4Cl_3(o\text{-}P_2)_3]PF_6$ ([**1**]PF_6), was obtained by slow diffusion of diethyl ether into the filtrate (90 mg, 94%). (Found: C 46.56, H 2.80, $C_{96}H_{78}F_6P_7Cl_3S_{16}Mo_3$ required C 46.48, H 2.95); $^{31}P\{^1H\}$ NMR (121.49 MHz, CD_2Cl_2): δ = 31.4 (s), 27.3 (s), −143.9 (sept, $^1J_{P-F}$ = 706 Hz); ESI(+)-MS *m*/*z* = 2324, $\mathbf{1}^+$.

$[Mo_3Se_4Cl_3(o\text{-}P_2)_3]PF_6$ ([2]PF_6). To a brown solution of $(PPh_4)_2[Mo_3Se_7Cl_4]$ (25 mg, 0.015 mmol) in CH_3CN (5 mL) was added a 5-fold-excess of PPh_3 (20 mg, 0.075 mmol) under nitrogen without apparent color change. After 2 h, *o*-P_2, (45 mg, 0.075 mmol) was added, and the solution was stirred overnight at room temperature to give a brown precipitate. After evaporation of the solvent, the resulting brown precipitate was redissolved in CH_2Cl_2, filtered and adsorbed onto a silica gel column. After washing of the column with acetone, elution with a KPF_6 solution in acetone (1 mg/mL) afforded a very concentrated brown solution. This solution was taken to dryness, redissolved in CH_2Cl_2, and filtered to remove the insoluble KCl or KPF_6 inorganic salts. Finally, an air stable microcrystalline brown solid, characterized as $[Mo_3Se_4Cl_3(o\text{-}P_2)_3]PF_6$ ([1]PF_6), was obtained by slow diffusion of diethyl ether into the filtrate (25 mg, 63%). (Found: C 45.56, H 3.06, $C_{96}H_{78}F_6P_7Cl_3S_{12}Se_4Mo_3$ required C 45.20, H 3.08); Raman IR ν_{max}/cm^{-1}; $^{31}P\{^1H\}$ NMR (121.49 MHz, CD_2Cl_2): δ = 35.5 (s), 21.5 (s), −143.9 (sept, $^1J_{P-F}$ = 706 Hz); ESI(+)-MS *m*/*z* = 2510, 2^+.

$[Mo_3S_4Cl_3(o\text{-}P_2)_3](PF_6)_4$ ([1]$(PF_6)_4$). To a brown-orange solution of [**1**]PF_6 (8 mg, 0.003 mmol) in CH_2Cl_2 (3 mL) at 0 °C was added a CH_2Cl_2/MeOH (7:3) solution of $NOPF_6$ (2.3 mg, 0.013 mmol) under nitrogen. The solution is completely dark green in 5 min, indicative of the presence of the $\mathbf{1}^{4+}$ cation. The resulting solution was taken to dryness to yield a green polycrystalline product characterized as [**1**]$(PF_6)_4$ (9.3 mg, 99%); (Found: C 38.35, H 2.60, $C_{96}H_{78}F_{24}P_{10}Cl_3S_{16}Mo_3$ required C 38.62, H 2.63); ESI(+)-MS *m*/*z* = 581.2, $\mathbf{1}^{4+}$; 823.2 $\{[\mathbf{1}^{4+} + PF_6]\}^{3+}$.

X-ray Crystallographic Study. The crystals were mounted on the tip of a glass fiber with the use of epoxi cement. X-ray diffraction experiments were carried out on a Bruker SMART CCD diffractometer for [**1**]$PF_6\cdot 2CH_2Cl_2$ and [**2**]$PF_6\cdot C_4H_{10}O\cdot CH_2Cl_2$, using Mo−Kα radiation (λ = 0.71073 Å) at 223 K. Data were collected with a frame width of 0.3° in ω and a counting time of 25 s per frame at a crystal to detector distance of 4 cm.

X-ray diffraction experiments for *o*-P_2=S were carried out on a Stoe Imaging Plate System using Mo−Kα radiation (λ = 0.71073 Å) at 293 K. The diffraction frames were integrated using the SAINT package and corrected for absorption with SADABS.[30] The structures were solved by direct methods and refined by the full-matrix method based on F^2 using the SHELXTL software package.[31] The crystal parameters and basic information relating data collection and structure refinement for monosulfurized *o*-P_2=S and compounds [**1**]$PF_6\cdot 2CH_2Cl_2$ and [**2**]$PF_6\cdot C_4H_{10}O\cdot CH_2Cl_2$ are summarized in Table 1.

Compound *o*-P_2=S crystallizes in the triclinic space group $P\bar{1}$, with one independent molecule in a general position in the unit cell. All non-H atoms were refined anisotropically, and hydrogen atoms were introduced at calculated positions (riding model), included in structure factor calculations but not refined. Compounds [**1**]$PF_6\cdot 2CH_2Cl_2$, and [**2**]$PF_6\cdot C_4H_{10}O\cdot CH_2Cl_2$ are isostructural and crystallize in the $P\bar{1}$ space group. All cluster and PF_6^- atoms were refined anisotropically while the positions of hydrogen from methyl and phenyl groups in the diphosphane ligands were generated geometrically, assigned isotropic thermal parameters, and allowed to ride on their respective parent carbon atoms. A number of highly disordered solvent molecules were found which were modeled as follows: for compound [**1**]$PF_6\cdot 2CH_2Cl_2$, four independent dichloromethane molecules were found and refined isotropically as rigid groups. Their occupancies were also refined yielding a 0.75 occupancy for CH_2Cl_2 molecules centered at C(100) and C(200) and 0.25 for those centered at C(300) and C(400). Hydrogen atoms of CH_2Cl_2 molecules were not included in the refinement. For compound [**2**]$PF_6\cdot C_4H_{10}O\cdot CH_2Cl_2$, one diethylether molecule was located, refined isotropically under rigid conditions, and its hydrogen atoms geometrically generated. Additionally, two independent dichloromethane molecules were found and refined

(30) (a) *SAINT 5.0*; Bruker Analytical X-Ray Systems: Madison, WI, 1996; (b) Sheldrick, G. M. *SADABS, empirical absorption program*; University of Göttingen: Göttingen, Germany, 1996.

(31) Sheldrick, G. M. *SHELXTL, 5.1*; Bruker Analytical X-Ray Systems: Madison, WI, 1997.

isotropically as rigid groups. Their occupancies were also refined yielding a 0.75 occupancy for CH_2Cl_2 molecules centered at C(300) and 0.25 for those centered at C(400). Hydrogen atoms of CH_2Cl_2 molecules were not included in the refinement.

Computational Methods

All calculations were carried out using the ADF 2005 program.[32] All species studied were optimized starting from the X-ray structure using DFT calculations, in particular the BP86 generalized gradient approximation, triple-ξ plus polarization Slater-type orbital basis sets,[33] (BP86/VTZP), and a fine mesh for numerical integration of the matrix elements. Large frozen cores (Mo·4p, Cl·2p, S·2p, P·2p, C·1s) were employed. Relativistic effects are considered using the ZORA formalism.[34]

Results and Discussion

***o*-P_2 Coordination to Mo_3Q_4 (Q = S, Se) Clusters: Synthesis and Crystal structure of [1]PF_6 and [2]PF_6.** The most convenient and rational approach to obtain $Mo_3(\mu_3\text{-}Q)(\mu\text{-}Q)_3$ (hereafter named as Mo_3Q_4; Q = S, Se) clusters bearing diphosphane ligands consists in the reaction of $Mo_3(\mu_3\text{-}Q)(\mu\text{-}Q_2)_3$-based clusters (hereafter named as Mo_3Q_7), typically starting from the polymeric phases $\{Mo_3Q_7Cl_4\}_n$ or the molecular $[Mo_3Q_7Cl_6]^{2-}$ dianions, with the appropriate phosphane ligand. This process implies the reduction of the Q_2^{2-} dichalcogenide bridges present in Mo_3Q_7 clusters to Q^{2-} chalcogenides in Mo_3Q_4. Fedin et al. first reported the synthesis of diphosphane-containing $[Mo_3Se_4Cl_3(dppe)_3]Cl$ and $[W_3Se_4Br_3(dppe)_3]Br$ complexes by reaction of the polymeric $\{Mo_3Se_7Cl_4\}_n$ phase or the molecular $[W_3Se_7Br_6]^{2-}$ dianion, respectively with an excess of dppe.[28,35] Later on, we comprehensively investigated this synthetic methodology pointing out that the solvent plays a crucial role in the excision of polymeric $\{Mo_3Q_7Cl_4\}_n$ (Q = S, Se) phases with diphosphanes, the reaction in boiling acetonitrile with reaction times close to 48 h being a general route for the preparation of complexes with formula $[Mo_3Q_4Cl_3(diphos)_3]^+$ according to reaction 1.[23,24] The generality of this procedure has been further illustrated by using different diphosphanes decorated with functional groups furnishing chirality or water solubility to the Mo_3Q_4 clusters.[36]

$$\{Mo_3Q_7Cl_4\}_n + 9/2\ \text{diphosphane} \rightarrow [Mo_3Q_4Cl_3(diphos)_3]Cl + 3/2\ \text{diphosphane(Q)}_2 \quad (1)$$

Initially, we attempted to extend this general route to the coordination of the TTF-functionalized *o*-P_2 diphosphane, although all attempts to coordinate this ligand to the trinuclear Mo_3S_4 unit starting from the polymeric $\{Mo_3S_7Cl_4\}_n$ or the $[Mo_3S_7Cl_6]^{2-}$ dianion in boiling acetonitrile were unsuccessful as evidenced by the dominant presence of the initial cluster and the *o*-P_2 ligand in the reaction media. Besides the starting materials, the only characterizable product was the monosulfurized *o*-P_2═S diphosphane isolated by silica-gel chromatography and characterized spectroscopically and by single crystal X-ray diffraction methods (see Supporting Information, Figure S1). A similar sulfurized dithiafulvenylphosphane ligand has been prepared by oxidation with S_8 in dichloromethane and structurally characterized.[18] We believe that the low basicity of the *o*-P_2 ligand prevents bridging S_2^{2-} disulfide reduction in Mo_3S_7 clusters to afford S^{2-} sulfides, thus avoiding the formation of Mo_3S_4 phosphane clusters. Thus, an alternative strategy was necessary to coordinate *o*-P_2 to these Mo_3S_4 cluster units. We decided to first reduce the S_2^{2-} ligands in $[Mo_3S_7Cl_6]^{2-}$ to afford soluble forms of the molecular Mo_3S_4 complexes and subsequently coordinate the *o*-P_2 ligand. For this purpose, we reacted the $[Mo_3S_7Cl_6]^{2-}$ dianion with a 5-fold excess of PPh_3, the progressive formation of a green solution characteristic of Mo_3S_4 complexes being observed.[29] It has been previously reported that the interaction of $\{Mo_3Se_7Cl_4\}_n$ with PEt_3 in methanol most likely produces a mixture of Mo_3Se_4 complexes with coordinated methanol, PEt_3, and halide ligands based on its subsequent reactivity.[37] By analogy with these results, we postulate that a mixture of complexes of general formula $[Mo_3Q_4(PPh_3)_xCl_y(solv)_z]^{(4-y)+}$ is obtained after treatment of $[Mo_3S_7Cl_6]^{2-}$ with PPh_3. Addition of *o*-P_2 to this solution yields after chromatographic workup, the corresponding hybrid molecular complex $[Mo_3S_4Cl_3(o\text{-}P_2)_3]PF_6$ ([**1**]PF_6) (see Scheme 2). Taking advantage of the easy availability of the selenium $[Mo_3Se_7Cl_6]^{2-}$ dianion, we have adapted the synthesis of [**1**]PF_6 to prepare the Se homologue, namely, $[Mo_3Se_4Cl_3(o\text{-}P_2)_3]PF_6$ ([**2**]PF_6), by reacting $[Mo_3Se_7Cl_6]^{2-}$ with PPh_3 and *o*-P_2 according to Scheme 2.

Both [**1**]PF_6 and [**2**]PF_6 were obtained in moderate yields (94% for [**1**]PF_6 and 63% for [**2**]PF_6). Compounds [**1**]PF_6 and [**2**]PF_6 are conveniently identified in solution by $^{31}P\{^1H\}$ where two phosphorus resonances at about δ = 28 and 24 ppm for [**1**]PF_6 and 31 and 21 ppm for [**2**]PF_6 are observed in agreement with a C_3-symmetrized cluster environment.[24,38] Further support on the integrity of compounds [**1**]PF_6 and [**2**]PF_6 is provided by ESI mass spectrometry where the $\mathbf{1}^+$ (m/z = 2324) and $\mathbf{2}^+$ (m/z = 2510) cations are observed as the base peaks in their respective spectra.

Single crystal X-ray diffraction studies reveal that compounds [**1**]PF_6 and [**2**]PF_6 are isostructural and crystallize in the triclinic $P\bar{1}$ space group. This space group does not have crystallographically imposed C_3 symmetry; however, the small deviations in the intermetallic distances for [**1**]PF_6 and [**2**]PF_6 are indicative of C_3 symmetrized complexes. The molecular structure of the $\mathbf{1}^+$

(32) Velde, G. T.; Bickelhaupt, F. M.; Baerends, E. J.; Guerra, C. F.; Van Gisbergen, S. J. A.; Snijders, J. G.; Ziegler, T. *J. Comput. Chem.* **2001**, *22*, 931.
(33) (a) Becke, A. D. *Phys. Rev. A* **1988**, *38*, 3098. (b) Perdew, J. P. *Phys. Rev. B* **1986**, *33*, 8822.
(34) (a) Vanlenthe, E.; Baerends, E. J.; Snijders, J. G. *J. Chem. Phys.* **1993**, *99*, 4597. (b) Vanlenthe, E.; Baerends, E. J.; Snijders, J. G. *J. Chem. Phys.* **1994**, *101*, 9783. (c) Vanlenthe, E.; Snijders, J. G.; Baerends, E. J. *J. Chem. Phys.* **1996**, *105*, 6505.
(35) Fedin, V. P.; Sokolov, M. N.; Myakishev, M. N.; Gerasko, A. O.; Fedorov, V. Y. *Polyhedron* **1991**, *10*, 1311.
(36) (a) Feliz, M.; Guillamon, E.; Llusar, R.; Vicent, C.; Stiriba, S. E.; Perez-Prieto, J.; Barberis, M. *Chem.—Eur. J.* **2006**, *12*, 1486. (b) Algarra, A. G.; Basallote, M. G.; Fernandez-Trujillo, M. J.; Guillamon, E.; Llusar, R.; Segarra, M. D.; Vicent, C. *Inorg. Chem.* **2007**, *46*, 7668.
(37) Saito, T.; Kajitani, Y.; Yamagata, T.; Imoto, H. *Inorg. Chem.* **1990**, *29*, 2951.
(38) Cotton, F. A.; Llusar, R.; Eagle, C. T. *J. Am. Chem. Soc.* **1989**, *111*, 4332.

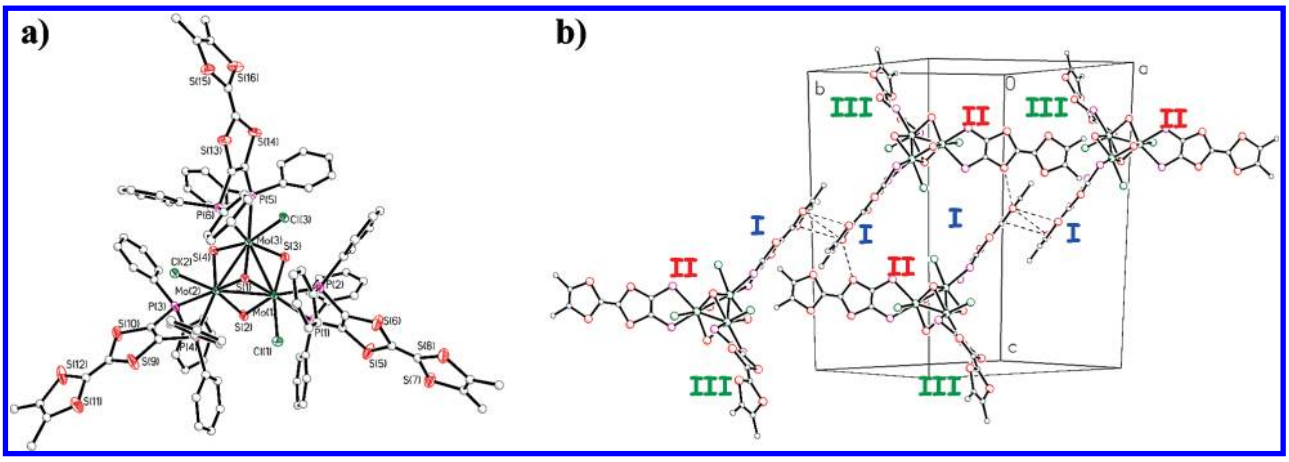

Figure 1. (a) ORTEP plot (50% thermal probability ellipsoids) of the $[Mo_3S_4Cl_3(o\text{-}P_2)_3]^+$ ($\mathbf{1}^+$) cation; carbon atoms are drawn as spheres for clarity; (b) crystal packing of compound [**1**]PF_6 with the o-P_2 numbering (I, II, and III) scheme and TTF close contacts (S···S below 4 Å); phenyl groups are omitted for clarity.

Table 2. Selected Bond Distances and Folding Angles for $[Mo_3S_4(o\text{-}P_2)_3Cl_3]PF_6\cdot 2CH_2Cl_2$ ($\mathbf{1}\cdot 2CH_2Cl_2$) and $[Mo_3Se_4(o\text{-}P_2)_3Cl_3]\cdot CH_2Cl_2\cdot C_4H_{10}O$ ($\mathbf{2}\cdot CH_2Cl_2\cdot C_4H_{10}O$)[a]

dist. (Å) and angles (deg)	$\mathbf{1}\cdot 2CH_2Cl_2$	$\mathbf{2}\cdot CH_2Cl_2\cdot C_4H_{10}O$
Mo−Mo range	2.7731(12)−2.7753(12)	2.8464(8)−2.8552(8)
Mo-(μ_3-Q) range	2.343(3)−2.354(3)	2.4692(8)−2.4801(8)
Mo-(μ-Q)[b] range	2.298(3)−2.314(3)	2.4227(8)−2.4392(8)
Mo-(μ-Q)[c] range	2.277(3)−2.280(3)	2.3966(8)−2.4042(9)
Mo−Cl range	2.470(2)−2.474(3)	2.4764(16)−2.4832(16)
folding along the P··P hinge (θ_1)	o-P2(**I**) 20.5(3)−o-P2(**II**) 26.8(3)−o-P2(**III**) 23.6(3)	o-P2(**I**) 20.2(2)−o-P2(**II**) 26.0(2)−o-P2(**III**) 24.3(2)
folding along the S··S hinge (θ_2)	o-P2(**I**) 5.39(7)−o-P2(**II**) 15.79(6)−o-P2(**III**) 23.06(7)	o-P2(**I**) 4.61(13)−o-P2(**II**) 16.71(14)−o-P2(**III**) 28.81(11)

[a] Mo−μ-Q distance *trans* to Mo−P(2) bond. [b] Mo−μ-Q distance *trans* to Mo−Cl. [c] Mo−μ-Q distance *trans* to Mo-μ-S.

cation is depicted in Figure 1a. Table 2 summarizes the most relevant bond distances for these complexes.

Each molybdenum atom in $\mathbf{1}^+$ (also applicable to $\mathbf{2}^+$) presents a pseudooctahedric coordination environment, with two out of three external positions being occupied by the phosphorus atoms of the o-P_2 ligand, one trans to the (μ_3-Q), and another trans to the (μ-Q). The third position is occupied by a chlorine atom, which is situated *trans* to the remaining (μ-Q). The replacement of sulfur by selenium mainly affects the bond distances within the Mo_3Q_4 cuboidal core, the most significant variation being an increase of about 0.08 Å in the Mo−Mo bond distance, ascribed to the increased atomic radius of selenium.

Incomplete cubane-type Mo_3Q_4 clusters featuring alkyl or aryl diphosphane (dmpe or dppe) ligands appears as discrete entities in the solid state;[24,25,38,39] however, the nature of the outer TTF-functionalized ligands in [**1**]PF_6 and [**2**]PF_6 may play an important structural role because of the potential formation of short interligand S···S or ligand-cluster S···Q contacts between neighboring clusters. The involvement of sulfur atoms from the cluster core and the peripheral ligands in the formation of supramolecular structures in the solid state has also been previously observed for the C_3-symmetrized Mo_3S_7 clusters.[40]

The crystal packing of [**1**]PF_6 and [**2**]PF_6 can be rationalized by considering the distinctive participation of the three non-crystallographically equivalent o-P_2 ligands in short contacts with neighboring clusters. Hence, dimerization between coplanar crystallographically equivalent o-P_2(I) ligands (those defined by the phosphorus P1−P2) occurs in the solid state through short S···S contacts (typically below 4.0 Å) between the sulfur atoms from the outer five-membered ring of one o-P_2(I) ligand and its crystallographically equivalent ligand belonging to a neighbor cluster. These interactions, (illustrated in Figure 1b for the $\mathbf{1}^+$ cation) formally result in dimers of trimers in the solid state with a minimum plane-to-plane distance of 3.595(6) Å (for $\mathbf{1}^+$) and 3.509(5) (for $\mathbf{2}^+$). These dimers are further connected through intermolecular S···S contacts between non-coplanar o-P_2(I) and o-P_2(II) (those defined by the phosphorus P3−P4) ligands (angle between the plane defined by the TTF skeleton 85.6(5)° for $\mathbf{1}^+$ and 87.4(3)° for $\mathbf{2}^+$) defining a two-dimensional (2D) network across the bc plane. The o-P_2(III) ligands (those defined by the phosphorus P5−P6) remain non-interacting in the solid state. We believe that the significant steric hindrance provided by the phenyl groups prevents a closer stacking of the TTF units.

Another structural feature of cations $\mathbf{1}^+$ and $\mathbf{2}^+$ is that the MoP_2C_2 metallacycle is folded along the P··P hinge (θ_1) in the 20.5(3)−26.8(3) range for $\mathbf{1}^+$ and 20.2(2)−26.0(2) range for $\mathbf{2}^+$ with no clear tendencies on these values on going from o-P_2(**I**) to o-P_2(**III**). The five-membered ring of the TTF core directly linked to the P atoms is also folded along the S··S hinge (θ_2) by 5.39(7) (for $\mathbf{1}^+$) and 4.61(13) (for $\mathbf{2}^+$) for the dimerized o-P_2(**I**) ligand. This value is significantly increased for o-P_2(**II**) 15.79(6)

(39) Llusar, R.; Sorribes, I.; Vicent, C. *Inorg. Chem.* **2009**, *48*, 4837.
(40) (a) Garriga, J. M.; Llusar, R.; Uriel, S.; Vicent, C.; Usher, A. J.; Lucas, N. T.; Humphrey, M. G.; Samoc, M. *Dalton Trans.* **2003**, 4546. (b) Llusar, R.; Uriel, S.; Vicent, C.; Clemente-Juan, J. M.; Coronado, E.; Gómez-Garcia, C. J.; Braida, B.; Canadell, E. *J. Am. Chem. Soc.* **2004**, *126*, 12076. (c) Alberola, A.; Llusar, R.; Triguero, S.; Vicent, C.; Sokolov, M. N.; Gomez-Garcia, C. *J. Mater. Chem.* **2007**, *17*, 3440.

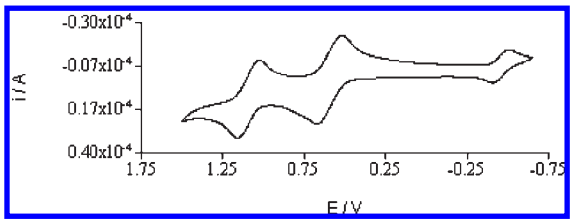

Figure 2. Cyclic voltammogram for compounds [**1**]PF_6 in CH_2Cl_2 at a scan rate of 500 mV s^{-1}.

(for $\mathbf{1}^+$) and 16.71(14) (for $\mathbf{2}^+$) and the non-interacting *o*-P_2(**III**) 23.06(3) (for $\mathbf{1}^+$) and 28.11(11) (for $\mathbf{2}^+$). Such folding angles (θ_1 and θ_2) are not unprecedented in the solid state for metal coordinated *o*-P_2 ligands and TTF donors and have already been observed in a number of transition metal complexes bearing TTF-functionalized diphosphane ligands,[4,15] thus illustrating the flexibility of the TTF core.

Electrochemistry

Mo_3Q_4 clusters are electron precise with six metal electrons, a formal +4 oxidation state for the molybdenum atoms, and are known to undergo rich electrochemical activity upon reduction. For example, the electrochemical behavior of the complexes $[Mo_3Q_4(dppe)_3Cl_3]PF_6$ (where formally the TTF framework of the *o*-P_2 ligand has been replaced by an ethylene bridge at parity of phenyl groups at the P atoms) exhibits a reversible process centered at about $E_{1/2} = -0.5$ V (vs Ag/AgCl). This process has been tentatively assigned to the two-electron reduction of the cluster core involving the couple $Mo^{IV}{}_3Q_4/Mo^{IV}$-$Mo^{III}{}_2Q_4$.[25] Regarding the TTF-based ligands, two reversible one-electron redox processes are observed for the free *o*-P_2 ligand at $E_{1/2} = 0.46$ and 0.91 V (vs Ag/AgCl). To investigate the effect of covalently associating *o*-P_2 ligands to the Mo_3Q_4 cluster cores, the redox properties of clusters [**1**]PF_6 and [**2**]PF_6 have been studied by cyclic voltammetry. Cyclic voltammograms of [**1**]PF_6 and [**2**]PF_6 performed in dichloromethane (see Figure 2) exhibit a reduction wave at $E_{1/2} = -0.46$ V (for $\mathbf{1}^+$) and $E_{1/2} = -0.48$ V (for $\mathbf{2}^+$) (vs Ag/AgCl) which is associated to the reduction of the Mo_3Q_4 cluster core. Two oxidation waves are also observed that correspond to the generation of the radical cation and the dication involving the TTF skeleton at $E_{1/2} = 0.58$ V and $E_{1/2} = 1.05$ V, respectively. A comparison of the peak currents for both waves suggests that the first and the second oxidation involve identical oxidation process that can be assigned to the couples $[Mo_3Q_4Cl_3(o\text{-}P_2)_3]^{+}/^{4+}$ and then $[Mo_3Q_4Cl_3(o\text{-}P_2)_3]^{4+}/^{7+}$. Non-appreciable broadening of these oxidation waves indicated the absence of sizable intramolecular or intermolecular interactions between TTF moieties.

Upon *o*-P_2 complexation to Mo_3Q_4 clusters, the *o*-P_2 donors experience a significant anodic shift (115 and 220 mV for the first and second oxidation process, respectively) as compared with the free phosphanes oxidation potentials, a common observation for related *o*-P_2-containing metal complexes.[2] This implies a prominent interaction through space or through bond between the TTF core and the metallic fragment. To investigate in more detail the electronic structures of these species, DFT calculations are reported in the next section.

Theoretical Analysis of the Molecular Orbital Diagram. To provide a better understanding on the nature of the active orbitals, DFT calculations at the BP86/VTZP level have been carried out on a model system of cation $\mathbf{1}^+$ where phenyl substituents and terminal methyl groups are replaced by hydrogen atoms, $\mathbf{1a}^+$. Full geometry optimization of $\mathbf{1a}^+$ yields bond distances and angles in reasonable agreement with X-ray results although bond distances are systematically enlarged because of the absence of the crystal environment. However, despite the overall C_3-symmetry of the model $\mathbf{1a}^+$ cluster, a low energetic cost is expected to be required for the folding of the MoP_2C_2 metallacycle along the P··P hinge (θ_1) of the diphosphane unit thus lowering such symmetry as it has been analyzed in other similar structures.[41] For this reason, folding angles of the ligands were not well reproduced most likely because of their strong dependence on three effects, namely, the bulky phenyl groups not considered in the calculation, on the specific intercluster interactions, and crystal packing forces. Inspection of the molecular orbital diagram (see Figure 3) reveals that the highest occupied molecular orbitals (HOMOs) are threefold-degenerate, corresponding to the π-system of individual (and isolated) TTF ligands. This picture is in contrast with previous analysis of molecular orbitals of dithiolate Mo_3S_7 clusters,[42] in which the π-systems of the three dithiolate ligands are combined through the metallic fragment. For the $\mathbf{1a}^+$ complex, the connection of TTF ligands to the metallic core through σ bonds of the phosphorus atoms avoids all possible bonding/antibonding combination with d-type orbitals available at molybdenum atoms, leading to well isolated TTF ligands with an excess of electronic charge in the π-system, a behavior already observed, for example, in [(*o*-P_2)$M(CO)_4$] (M = Mo, W) complexes.[19]

Chemical and Electrochemical Oxidation of Compounds [1]PF_6 and [2]PF_6. The two-step chemical or electrochemical oxidation of TTF and its derivatives offers the possibility of controlling the production of neutral, radical cation, or dication in solution with the aim of developing new molecular materials with applications such as molecular switches, non linear optical materials, or the preparation of supramolecular systems.[43] Moreover, solid state chemistry of TTF-based donors have also attracted much interest, especially for the development of new organic metals and superconductors.[44] An interesting class of TTF-based materials is that comprising compounds featuring multiple TTF moieties arranged in highly symmetrical environments by using different platforms. For example, the study of hexaquis-TTF

(41) Frantz, R.; Guillamón, E.; Lacour, J.; Llusar, R.; Polo, V.; Vicent, C. *Inorg. Chem.* **2007**, *46*, 10717.
(42) Llusar, R.; Triguero, S.; Polo, V.; Vicent, C.; Gomez-Garcia, C.; Jeannin, O.; Fourmigue, M. *Inorg. Chem.* **2008**, *47*, 9400.
(43) (a) Jorgensen, T.; Hansen, T. K.; Becher, J. *Chem. Soc. Rev.* **1994**, *23*, 41. (b) Batail, P.; Boubekeur, K.; Fourmigue, M.; Gabriel, J.-C. *Chem. Mater.* **1998**, *10*, 3005. (c) Bryce, M. R.; Devonport, W.; Goldenberg, L. M.; Wang, C. *Chem. Commun.* **1998**, 945. (d) Bryce, M. R. *J. Mater. Chem.* **2000**, *10*, 589. (e) Nielsen, M. B.; Lomholt, C.; Becher, J. *Chem. Soc. Rev.* **2000**, *29*, 153. (f) Segura, J. L.; Martin, N. *Angew. Chem., Int. Ed.* **2001**, *40*, 1372.
(44) (a) Williams, J. M.; Ferraro, J. R.; Thorn, R. J.; Carlson, K. D.; Geiser, U.; Wang, H. H.; Kini, A. M.; Whangbo, M. H., *Organic Superconductors*. Prentice Hall: Upper Saddle River, NJ, 1992; (b) Day, P.; Kurmoo, M. *J. Mater. Chem.* **1997**, *8*, 1291. (c) Batail, P. *Chem. Rev.* **2004**, *104*, 4887.

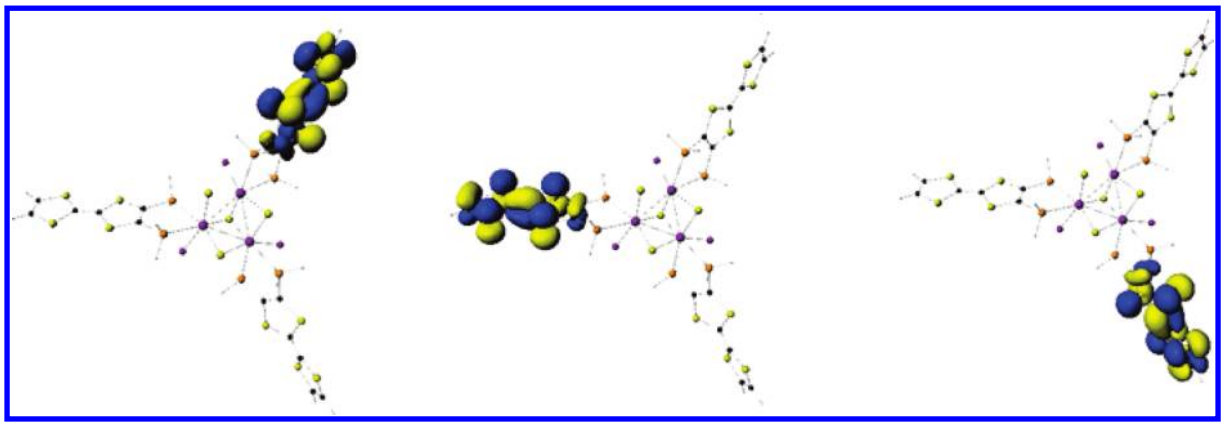

Figure 3. Representation of the three HOMOs of $\mathbf{1a}^{+}$ complex calculated at the DFT level.

donors with hexagonal symmetry relies on the use of all-functionalized benzene as platform,[45] whereas C_3-symmetrized TTF trimers typically relies on the use of 1,3,5 substituted benzene moieties,[26] or tris-annulated macrocycles.[46] Another interesting example has been recently reported by Coulon and Batail with the preparation of the $(EDT\text{-}TTF\text{-}CONH_2)_2[Re_6Se_8(CN)_6]$ salt, an organic−inorganic system where the amide-functionalized TTF donor expresses the 3-fold symmetry of the inorganic cluster anion.[47]

The interest of these highly symmetrical molecules is 2-fold: (i) on one side, they inherently possess degenerate frontier orbitals, and (ii) on the other side, they may be involved in distinctive intra- or intermolecular interactions modulated by their molecular symmetry, leading to highly symmetrized networks in the solid state. Regarding cluster based platforms, correlations between molecular geometry and network symmetry have been recently highlighted by DiSalvo's group for the octahedrally symmetrized $W_6S_8((TTF)PEt_2)_6$ complex which assembles in closest packings in the solid state, where each molecule maintains good intermolecular contacts with multiple closest neighbors mainly dictated by the O_h symmetry of the molecular cluster.[21] In this context, we believe that cations $\mathbf{1}^{+}$ and $\mathbf{2}^{+}$, with TTF "arms" around a C_3-symmetrized Mo_3Q_4 platform held together by phosphorus linkage, are interesting targets for the study of their oxidation chemistry. For this purpose we have undertaken an investigation of the chemical or electrochemical oxidation of compounds $\mathbf{1}^{+}$ and $\mathbf{2}^{+}$ both in solution and in the solid state.

Solution Speciation upon Oxidation. Oxidation reactions of compounds $[\mathbf{1}]PF_6$ and $[\mathbf{2}]PF_6$ using $NOPF_6$ as oxidant were monitored in situ by ESI-MS. This technique has proved to be a convenient tool for the characterization of Mo_3Q_4 clusters featuring diphosphanes,[48] and also to confirm the presence of each of the intermediates during the oxidation of multi TTF-containing compounds.[49] ESI mass spectra (see Figure 4) of the reaction of complex $[\mathbf{1}]PF_6$ with $NOPF_6$ reveal an immediate decrease of the signal of the $\mathbf{1}^{+}$ cation (m/z = 2324.7) concomitant with the formation of doubly and triply charged species and a color change from orange to green. These multiply charged species were identified as $\mathbf{1}^{2+}$ (m/z = 1162.4), $\mathbf{1}^{3+}$ (m/z = 774.6), $[\mathbf{1}^{3+} + PF_6]^{2+}$ (m/z = 1234.8), $[\mathbf{1}^{4+} + PF_6]^{3+}$ (m/z = 823.2), and minor signals of the $\mathbf{1}^{4+}$ cation (m/z = 581.2) as judged by both the mass-to-charge ratio and the isotopic pattern (see Supporting Information, Figure S2). The identity of these cations gives support to the sequential formation of the oxidized $\mathbf{1}^{2+}$, $\mathbf{1}^{3+}$, and $\mathbf{1}^{4+}$ species in solution as the amount of oxidant is increased.

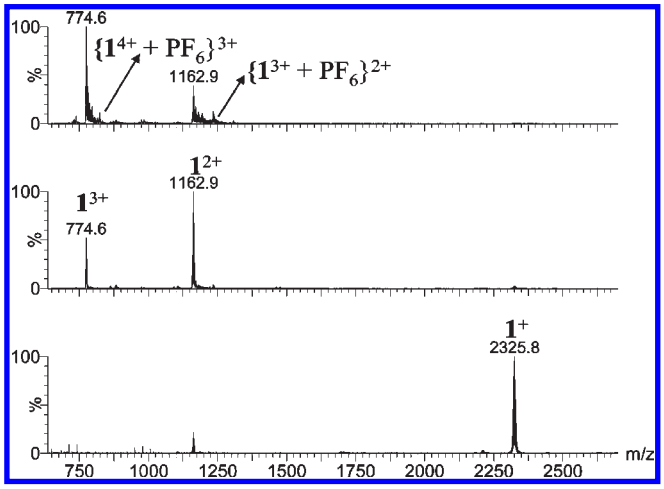

Figure 4. ESI mass spectrum of acetonitrile solutions of $[\mathbf{1}]PF_6$ (bottom) and ESI mass spectra of the reaction of compound $[\mathbf{1}]PF_6$ with a increasing amounts of $NOPF_6$ (middle and top).

The presence of higher aggregates (dimers or trimers) based on Mo_3Q_4 clusters in solution was not evidenced as judged by ESI-MS, even after using different Mo_3Q_4 cluster concentrations for the ESI-MS analysis (at concentrations up to 1×10^{-3} M); however, ESI-MS analysis revealed a slow side reaction associated to the oxidation with $NOPF_6$ that consists in the partial Cl to F replacement in the Mo_3Q_4 cluster core most likely from halide scrambling of the PF_6^{-} counteranion as previously found

(45) (a) Christiansen, C. A.; Bryce, M. R.; Batsanov, A. S.; Becher, J. *Chem. Commun.* **2000**, 331. (b) Hasegawa, M.; Enozawa, H.; Kawabata, Y.; Iyoda, M. *J. Am. Chem. Soc.* **2007**, *127*, 3072.

(46) Akutagawa, T.; Abe, Y.; Hasegawa, T.; Nakamura, T.; Inabe, T.; Sugiura, K.-I.; Christiansen, C. A.; Lau, J.; Becher, J. *J. Mater. Chem.* **1999**, *9*, 2737.

(47) Baudron, S. A.; Batail, P.; Coulon, C.; Clerac, R.; Canadell, E.; Laukhin, V.; Melzi, R.; Wzietek, P.; Jerome, D.; Auban-Senzier, P.; Ravy, S. *J. Am. Chem. Soc.* **2005**, *127*, 11785.

(48) Guillamon, E.; Llusar, R.; Pozo, O.; Vicent, C. *Int. J. Mass Spectrom.* **2006**, *254*, 28.

(49) Chiang, P.-T.; Chen, N.-C.; Lai, C.-C.; Chiu, S.-H. *Chem.—Eur. J.* **2008**, *14*, 6546.

Table 3. Redox Potentials and Spectroscopic Data in CH_2Cl_2 (ca. 5×10^{-4} M) of *o*-P_2, [**1**]PF_6, [**2**]PF_6, and Their Oxidized Counterparts *o*-$P_2(PF_6)$, [**1**]$(PF_6)_4$ and [**2**]$(PF_6)_4$[a]

compound	λ_{abs}/nm ($\varepsilon/10^3$ dm^3 mol^{-1} cm^{-1})	oxidation $E_{1/2}$ (ΔE^c)/V	oxidation $E_{1/2}$ (ΔE^c)/V	reduction $E_{1/2}$ (ΔE^c)/V
o-P_2	273(10.7), 322(6.8), 424(0.8)	0.91(65)	0.46(69)	
o-$P_2(PF_6)$	263(6.3), 339(2.3), 447(1.8), 622 (0.9)			
[**1**]PF_6	271(30.2), 319(22.4), 415(5.5), 628(0.6)	1.14(65)	0.58(68)	−0.46(64)
[**2**]PF_6	271(27.6), 317(15.8), 372(5.4), 654(0.6)	1.12(67)	0.55(70)	−0.48(67)
$[Mo_3S_4(dppe)_3Cl_3]PF_6$	279(16), 357(8.5), 409(7.9), 643 (0.6)			−0.50(68)
$[Mo_3Se_4(dppe)_3Cl_3]PF_6$	292(8.0), 375(5.4), 445(5.1), 693 (0.6)			−0.52(78)
[**1**]$(PF_6)_4$	264(30.0), 324(12.1), 400(4.7), 634(0.6)			
[**2**]$(PF_6)_4$	268(28.9), 331(10.8), 452(4.0), 645 (0.7)			

[a] Referenced to Fc/Fc^+ at $E_{1/2} = 0.44$ V (vs Ag/AgCl). [b] $\Delta E = |E_a - E_c|$ in mV.

for W_3S_4 closely related complexes.[50] Nevertheless, the identity of the Mo_3Q_4 core featuring *o*-P_2 diphosphanes remains unchanged, thus suggesting a remarkable stability. The addition of more than 4 equiv of $NOPF_6$ leads to diphosphane decoordination as evidenced by the presence of a prominent peak at $m/z = 600$ corresponding to the free *o*-P_2.

To evaluate the influence of the coordination on the electronic properties of the *o*-P_2 ligand and the Mo_3Q_4 cluster core, the absorption UV−vis spectra of the ligand *o*-P_2 and compounds [**1**]PF_6 and [**2**]PF_6 were compared. The electronic spectra of compounds *o*-P_2, [**1**]PF_6 and [**2**]PF_6 are very much alike in the high energy region (typically below $\lambda = 400$ nm) and reveal two intense high energy bands, with maxima at about 270 and 320 nm, respectively, consistent with absorptions from neutral TTF moieties. Additional low energy bands are observed for [**1**]PF_6 and [**2**]PF_6 at $\lambda = 628$ and 654 nm, respectively, which are characteristic of the Mo_3Q_4 chromophore. For comparative purposes, the absorption UV−vis spectra of the $[Mo_3Q_4Cl_3(dppe)_3]PF_6$ homologues, lacking of TTF-based ligands, were also studied (see Table 3). In general, the anchorage of the ligands onto the Mo_3Q_4 cluster core does not lead to new bands, as can be anticipated from DFT calculations. As illustrated in Figure 5a, complex $\mathbf{1}^+$ absorbs similarly to that of $[Mo_3S_4Cl_3(dppe)_3]PF_6$ and the free ligand, thus affording a characteristic UV−vis spectrum that can be interpreted in terms of simple superposition of the electronic transitions of the two constituents.

Upon oxidation of the *o*-P_2 ligand with 0.5 or 1 equiv of $NOPF_6$, we noticed minor shifts of the two highest energy absorptions but significant variations in their relative intensities (see Table 3). Moreover, we observed the emergence of two bands assigned to isolated (non-interacting) TTF cation radicals (λ_{max} 447 and 622 nm) and the lack of neither the low energy absorption band of interacting TTF cation radicals ($\pi-\pi$ dimers)[51,52] at about λ_{max} 850 nm nor mixed valence bands typically observed at 2000 nm for pairs of stacked TTF units.[51,53] UV−visible-near-infrared (UV−vis−NIR) investigation was also carried out for complexes [**1**]PF_6 and [**2**]PF_6 by a successive aliquot addition of $NOPF_6$. Chemical oxidation of [**1**]PF_6 by increasing (up to three) equivalents of $NOPF_6$ was accompanied by a color change from orange to green. The UV−vis spectrum clearly changed, the original high energy absorptions being slightly shifted accompanied by a large change in their relative intensity in a similar way to that found for the couple *o*-P_2/*o*-P_2^+. The appearance of new bands assigned to isolated (non-interacting) TTF cation radicals (λ_{max} 447 and 622 nm) was not clearly observed because of the overlapping with those bands due to the cluster core. A broadening of the low energy absorption of the Mo_3Q_4 core ($\lambda_{max} = 628$ for [**1**]PF_6 and 654 for [**2**]PF_6) evidenced the characteristic absorption at $\lambda_{max} = 622$ typical of the isolated TTF cation radical. As expected, the maximum broadening for this band is obtained with 3 equiv of the oxidizing agent. Like the couple *o*-P_2/*o*-P_2^+, absorption UV−vis spectroscopy suggests the absence of sizable intermolecular mixed-valence species in solution for [**1**]PF_6 and [**2**]PF_6 during the addition of 1 or 2 equiv of $NOPF_6$. These observations are further supported by EPR studies on chemically or electrochemically oxidized samples of [**1**]PF_6, which showed only a very broad and intense signal, centered at $g = 2.0079$, characteristic of the isolated TTF radical cations (see Supporting Information, Figure S3). The absence of any hyperfine structure very likely indicates a dynamic behavior in solution of the oxidized species, thus precluding any observation of the coupling of the unpaired electrons with the Me groups protons and the phosphorus nuclei. Moreover, no variation of the signal with the amount of added oxidant was observed.

Solid State Characterization of Oxidation Products from [1]PF_6 and [2]PF_6. As pointed out above, oxidation of the molecular [**1**]PF_6 and [**2**]PF_6 hybrids with increasing amounts of $NOPF_6$ produces the multiply charged $[\mathbf{1}]^{n+}$ and $[\mathbf{2}]^{n+}$ ($n = 1-4$) species in solution. We face the preparation and isolation of salts of general formula [**1**]$(PF_6)_4$ and [**2**]$(PF_6)_4$ by adding a 3-fold excess of $NOPF_6$ to dichlroromethane solutions of the corresponding [**1**]PF_6 and [**2**]PF_6 cations (see Experimental Section), leading to a microcrystalline green powder. All attempts to obtain single crystals of both [**1**]$(PF_6)_4$ and [**2**]$(PF_6)_4$ were unsuccessful. Experimental evidence of the preparation and isolation in analytically pure form of compound [**1**]$(PF_6)_4$ (and also applicable to [**2**]$(PF_6)_4$ was obtained by elemental analysis and Raman and solid state UV−vis spectroscopies. In general, Raman spectra of the TTF-based donors are known to reveal essential information on their oxidation state (for example for the BEDT-TTF[54] or BEDO-TTF),[55] the vibrational

(50) Vicent, C.; Feliz, M.; Llusar, R. *J. Phys. Chem. A* **2008**, *112*, 12550.
(51) Torrance, J. B.; Scott, B. A.; Welber, F. B. *Phys. Rev. B* **1979**, *19*, 730.
(52) Khodorkovsky, V.; Shapiro, L.; Krief, P.; Shames, A.; Mabon, G.; Gorgues, A.; Giffard, M. *Chem. Commun.* **2001**, 2736.
(53) (a) Ziganshina, A. Y.; Ko, Y. H.; Jeon, W. S.; Kim, K. *Chem. Commun.* **2004**, 806. (b) Yoshizawa, M.; Kumazawa, K.; Fujita, M. *J. Am. Chem. Soc.* **2005**, *127*, 13456. (c) Rosokha, S. V.; Kochi, J. K. *J. Am. Chem. Soc.* **2007**, *129*, 828. (d) Kitahara, T.; Shirakawa, M.; Kawano, S.-I.; Beginn, U.; Fujita, N.; Shinkai, S. *J. Am. Chem. Soc.* **2005**, *127*, 14980.
(54) Wang, H. H.; Ferraro, J. R.; Williams, J. M.; Geiser, U.; Schlueter, J. A. *J. Chem. Soc., Chem. Commun.* **1994**, 1893.
(55) Drozdova, O.; Yamochi, H.; Yakushi, K.; Uruichi, M.; Horiuchi, S.; Saito, G. *J. Am. Chem. Soc.* **2000**, *122*, 4436.

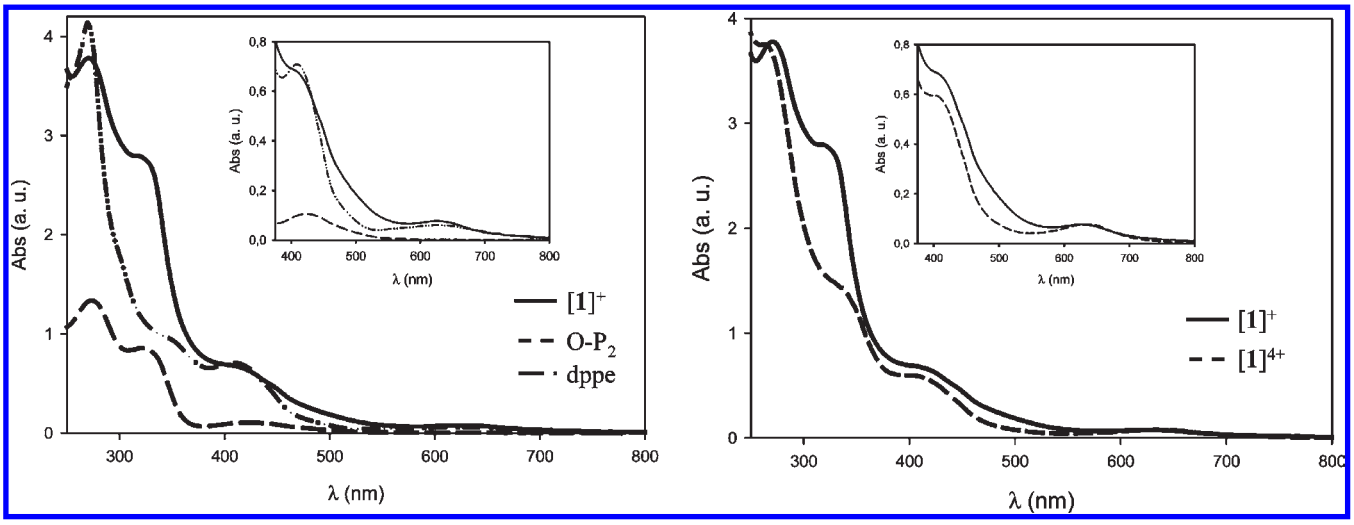

Figure 5. Absorption UV−vis spectra of 1×10^{-4} M dichloromethane solutions of compounds *o*-P_2, [**1**]PF_6 and $[Mo_3S_4Cl_3(dppe)_3]PF_6$ (left) and [**1**]PF_6 and [**1**]$(PF_6)_4$ (right).

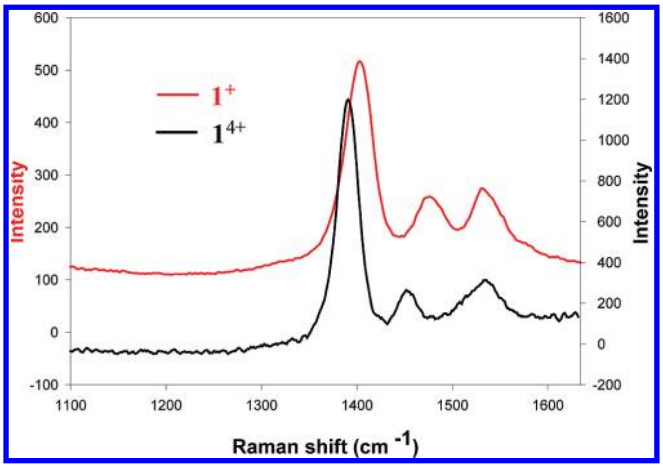

Figure 6. Raman spectrum of the redox couples and $\mathbf{1}^+$ and $\mathbf{1}^{4+}$ in the 1100 to 1630 cm^{-1} range.

frequencies of the C=C and C−S bands being sensitive probes for the oxidation state of the molecule. When electrons are removed from the HOMO, which has bonding characteristics with respect to the C=C bond, the C=C vibration frequencies decrease. Since the HOMO has antibonding characteristics with respect to the C−S bands, the effect of oxidation is strengthening of the C−S bonds and increase of the C−S frequencies.[54] The Raman spectrum for pure *o*-P_2 show three strong bands in the 1350−1600 cm^{-1} (1478, 1522, and 1568 cm^{-1}) range. An identical pattern is observed in the Raman spectrum of compounds [**1**](PF_6) and [**2**](PF_6), all bands being slightly shifted to lower wavenumbers as compared with the free *o*-P_2 (see Figure 6, bands at 1417, 1479, and 1546 cm^{-1}). The two lowest wavenumber are associated with the two C=C double bonds of the five-membered rings and the central C=C double bond, respectively (those at 1417 and 1479 cm^{-1}) of the TTF framework. The band at 1546 cm^{-1} remains almost unchanged on going from $\mathbf{1}^+$ to its oxidized form, and this band is also present in $[Mo_3S_4Cl_3(dppe)_3]PF_6$, thus suggesting that it involves the dppe backbone.[56] For compound $\mathbf{1}^{4+}$, the two lower wavenumber bands (see Figure 6) are shifted to lower values, which is a common observation on going from neutral to oxidized TTF-based donors.

UV−vis spectra also proved that oxidized *o*-P_2 ligands are present in solid state samples of [**1**]$(PF_6)_4$. A weak band centered at 650 nm was evidenced in a similar way to that observed in solution that corresponds to electron transfers between donor molecules with an integer charge. Two additional high energy bands are observed in the 250 to 350 nm range which are identical to those observed in the NIR−vis spectra of pure cluster [**1**]$(PF_6)_4$ and [**2**]$(PF_6)_4$ in solution.

Conclusions

The TTF−diphosphane $[Mo_3S_4Cl_3(o\text{-}P_2)_3]PF_6$ ([**1**]PF_6) complex was prepared in a two-step procedure starting from the molecular $[Mo_3S_7Cl_6]^{2-}$ dianion. In a first stage, the S_2^{2-} disulfide ligands in $(n\text{-}Bu_4N)_2[Mo_3S_7Cl_6]$ are reduced with PPh_3 to yield an intermediate featuring a Mo_3S_4 cluster core followed by in situ addition of the *o*-P_2 ligand that affords [**1**]PF_6 in high yield. The preparation of the selenium homologue, namely, $[Mo_3Se_4Cl_3(o\text{-}P_2)_3]PF_6$ ([**2**]PF_6), has been carried out analogously to that reported for the sulfur homologue, starting from $[Mo_3Se_7Cl_6]^{2-}$. Both [**1**]PF_6 and [**2**]PF_6 were characterized by $^{31}P\{^1H\}$ NMR, ESI mass spectrometry, and single-crystal X-ray crystallography. Regarding the electronic characteristics of [**1**]PF_6 and [**2**]PF_6, electrochemical studies and DFT calculations reveal the presence of two reversible oxidations associated with the three independent TTF ligands which further supports previous observations regarding a lack of TTF communication through the phosphane atoms in TTF-diphosphane ligands. The oxidation chemistry in solution indicates that the cationic $\mathbf{1}^{n+}$ (n = 1−4) species can be readily accessed by increasing the amounts of $NOPF_6$ (up to 3 equiv). Of particular interest is the solid state spectroscopic UV−vis and Raman characterization of the oxidized species formulated as [**1**]$(PF_6)_4$ which provide an input for spectroscopic signature of oxidized species in the still rare stable $\mathbf{1}^{4+}$ and $\mathbf{2}^{4+}$ species featuring TTF-oxidized ligands. For example, among TTF-pyridines, only one acetylacetonate metal complex has been successfully oxidized to afford cation radical salts,[13]

(56) Pikl, R.; Duschek, F.; Fickert, C.; Finsterer, R.; Kiefer, W. *Vib. Spectrosc.* **1997**, *14*, 189.

while only one example of TTF-phosphane metal complexes has been so far oxidized to the corresponding radical cation salts, namely, $[Mo(CO)_4(o\text{-}P_2]_2(Mo_6O_{19})$.[8]

It has to be pointed out that the coordination by covalent bonding of TTF-based diphosphanes to the Mo_3Q_4 cores constitutes an interesting class of hybrid organic−inorganic systems lying at the crossing of two research avenues: the advantages of TTF-based materials with those of inorganic clusters with possible synergetic effects between them. In our design, we wished to exploit building units of C_3-symmetrized Mo_3Q_4 clusters featuring three TTF ligands to promote intermolecular $\pi-\pi$ interactions through TTF cofacial stacking with the aim of creating systems whose geometric shape favors orbital interactions in more than one dimension. In this sense, work is in progress aimed at obtaining detailed structural information by X-ray diffraction methods of the oxidized $\mathbf{1}^{4+}$ and $\mathbf{2}^{4+}$ or partially $\mathbf{1}^{n+}$ and $\mathbf{2}^{n+}$ species as well as the effect of the counterions in the solid state ordering which ultimately will determine their physicochemical properties.

Acknowledgment. This work was supported by the Spanish Ministerio de Educación y Ciencia (MEC) (Project CTQ2005-09270-C02-01), Ministerio de Ciencia e Innovación (Projects CTQ2008-02670/BQU), and Fundació Bancaixa-Universitat Jaume I (Projects P1.1B2007-12). The authors also are grateful to the Serveis Centrals d'Instrumentació Científica (SCIC) of the Universitat Jaume I for providing us with mass spectrometry, NMR, and X-ray facilities, and a generous allotment of computer time. I.S. thanks the Spanish Ministerio de Ciencia e Innovación (MICINN) for a doctoral fellowship (FPU). Support from the CNRS and University of Angers is also acknowledged. The authors thank Prof. M. Geoffroy and Dr. P. Grosshans (University of Geneva, Switzerland) for EPR measurements.

Supporting Information Available: Crystallographic data (excluding structure factors) for the structures reported in this paper. Molecular structure of the monosulfurized $o\text{-}P_2{=}S$ ligand (Figure S1); observed and theoretical isotopic pattern for the multiply charged $\mathbf{1}^{2+}$, $\mathbf{1}^{3+}$, $[\mathbf{1}^{3+} + PF_6]^{2+}$, $[\mathbf{1}^{4+} + PF_6]^{3+}$, and $\mathbf{1}^{4+}$ (Figure S2) and EPR spectrum of $\mathbf{1}^{4+}$ (Figure S3). View of the optimized geometry for structure $\mathbf{1a}^+$ (Figure S4), selected bond distances and folding angles for $\mathbf{1a}^+$ BP86/VTZP optimized geometry (Table S1), and list of Cartesian coordinates (in Angstroms) for the BP86/VTZP optimized structure of $\mathbf{1a}^+$. This material is available free of charge via the Internet at http://pubs.acs.org.